Article:
Hunt, Neil Terrence, Lynam, Jason Martin, Procacci, Barbara et al. (2025) Ultrafast vibrational spectroscopic analysis of the ubiquitous precatalyst [Mn2(CO)10] in different solvents. Journal of Chemical Physics. 174302. ISSN: 1089-7690

https://doi.org/10.1063/5.0254482

The Journal of Chemical Physics

RESEARCH ARTICLE | MAY 01 2025

Ultrafast vibrational spectroscopic analysis of the ubiquitous precatalyst $[Mn_2(CO)_{10}]$ in different solvents

Special Collection: David Jonas Festschrift

Amy L. Farmer ; Barbara Procacci ; Daniel J. Shaw ; Sabina Gurung; Ian J. S. Fairlamb ; Jason M. Lynam ; Neil T. Hunt

J. Chem. Phys. 162, 174302 (2025)
https://doi.org/10.1063/5.0254482

The Journal of Chemical Physics ARTICLE pubs.aip.org/aip/jcp

Ultrafast vibrational spectroscopic analysis of the ubiquitous precatalyst [$Mn_2(CO)_{10}$] in different solvents

Cite as: J. Chem. Phys. 162, 174302 (2025); doi: 10.1063/5.0254482
Submitted: 23 December 2024 • Accepted: 8 April 2025 •
Published Online: 1 May 2025

Amy L. Farmer,[1] Barbara Procacci,[1,a)] Daniel J. Shaw,[1] Sabina Gurung,[1] Ian J. S. Fairlamb,[2] Jason M. Lynam,[2] and Neil T. Hunt[1]

AFFILIATIONS

[1] Department of Chemistry and York Biomedical Research Institute, University of York, York YO10 5DD, United Kingdom
[2] Department of Chemistry, University of York, York YO10 5DD, United Kingdom

Note: This paper is part of the JCP Special Topic, David Jonas Festschrift.
[a)] **Author to whom correspondence should be addressed:** barbara.procacci@york.ac.uk

ABSTRACT

Infrared (IR) absorption and time resolved IR (IR_{pump}–IR_{probe}, 2D-IR) spectroscopies have been combined to study the vibrational dynamics and solvent interactions of the carbonyl ligand stretching vibrational modes of the photocatalyst dimanganese decacarbonyl, [$Mn_2(CO)_{10}$], in solvents with varying physical properties (heptane, cyclohexane, THF, MeCN, DMSO, ^{i}PrOH, and MeOH). The presence of a solvent-mediated symmetry breaking mechanism leading to a gain in oscillator strength of formally symmetry-forbidden modes was observed in all solvents, although the effect was more marked in polar solvents. Ultrafast vibrational energy dissipation was found to occur *via* two solvent dependent relaxation pathways, rapid intramolecular vibrational energy redistribution (IVR ~ 0.3–1 ps) and relaxation to the ground vibrational state (T_1 ~ 80–250 ps). Accelerating factors for vibrational relaxation included hydrogen bonding and the presence of solvent vibrational modes resonant with the carbonyl modes of [$Mn_2(CO)_{10}$], while IVR timescales displayed an anticorrelation with vibrational relaxation times. Overall, a simple association of dynamic behavior with solvent properties could not be identified for any of the measured parameters. Rather, specific solvent properties were found to contribute to different extents in each case. Thus, our results highlight the need for careful consideration of solvent factors when attempting a rational selection of catalyst/solvent combinations or the implementation of sustainable replacement solvents.

INTRODUCTION

In recent years, much attention has focused on efforts to find replacements for catalysts comprising 4*d* and 5*d* organometallic species through the development of systems based on the more earth-abundant first row transition metals.[1–3] One prominent set of examples are the manganese carbonyl complexes, which have found applications for processes including C–H and C–X (X = halogen) bond activation.[4–12] Here, we focus on dimanganese decacarbonyl, [$Mn_2(CO)_{10}$], a precatalyst that has been used to promote the generation of new C–C bonds through photochemical[7–14] and thermal[15–26] pathways. In the photochemical reactions, visible wavelength irradiation proceeds to abstract a halogen atom from an alkyl halide, producing alkyl radicals, whereas in the thermal C–H bond functionalization reactions, the first step is CO-loss to form [$Mn_2(CO)_9$].[27] As in all cases of homogeneous catalysis, the solvation of the precatalyst and interactions of solvent molecules with any subsequently formed vacant coordination sites are likely to play a key role in determining the mechanism of the reaction and the rates of individual steps. This motivates the desire to understand the molecular level interactions of catalyst molecules with their solvation environment. In addition to informing our understanding of reaction mechanisms, such studies will also provide the fundamental insight needed to guide the replacement of traditional solvents with sustainable, green alternatives.

Infrared (IR) spectroscopy is a particularly valuable tool for the investigation of metal carbonyl complexes, owing to the structure-specific and environmentally sensitive nature of their carbonyl

ligand stretching vibrational modes (ν_{CO}), which occur near 2000 cm^{-1} in the mid-IR. Time-resolved IR (TR-IR) spectroscopies, employing pump–probe methodologies allow further details of molecular dynamics, energy relaxation, and bond formation to be obtained. Relevant examples include investigation of the structural, solvation, and orientational dynamics of transition metal carbonyls[28–40] and their photoproducts.[41–43]

In the case of $[Mn_2(CO)_{10}]$, reported time resolved studies fall into two categories. UV_{pump}–IR_{probe} experiments[44–49] (295–400 nm) identified wavelength dependent photochemical pathways, leading to the formation of $[Mn(CO)_5^{\cdot}]$ (longer wavelength) and $[Mn_2(CO)_9]$ (shorter wavelength), while IR-based pump–probe spectroscopies, including multidimensional techniques (2D-IR), focused on solvation dynamics.[50] Of particular relevance to our study, 2D-IR spectroscopy of $[Mn_2(CO)_{10}]$ in cyclohexane revealed a band assignment for the diagonal and off-diagonal 2D-IR peaks along with the observation of coherence transfer processes between ν_{CO} modes.[35,51–53] Orientational dynamics of $[Mn_2(CO)_{10}]$ were reported in cyclohexane,[28] while solvation of $[Mn_2(CO)_{10}]$ in a series of linear alcohols revealed the impact of changing solvent viscosity and the extent of solvent–solute hydrogen bonding.[35,52] Intermolecular and intramolecular energy dissipation timescales were determined to be on the order of hundreds and a few picoseconds, respectively, while the degree of hydrogen-bonding between solvent and solute was shown to correlate with longer intramolecular vibrational energy redistribution (IVR) timescales.[28,35,53] Spectral diffusion dynamics of the ν_{CO} modes of $[Mn_2(CO)_{10}]$ were found to be linked to solvent viscosity. Together, these studies led to a description of the ν_{CO} modes of $[Mn_2(CO)_{10}]$ using a vibrational aggregate model,[52,54] which invoked local frequency disorder distributions leading to a loss of symmetry and the presence of otherwise symmetry forbidden Raman modes in the $[Mn_2(CO)_{10}]$ spectra.

These detailed studies have elucidated the behavior of $[Mn_2(CO)_{10}]$ in specific solvents (of wider relevance to catalysis) and form a basis for the broader, comparative picture of the dynamics of $[Mn_2(CO)_{10}]$ in a range of solvents that we report here. In this context, we have combined IR absorption, IR_{pump}–IR_{probe}, and 2D-IR spectroscopy to investigate the solvation and dynamics of $[Mn_2(CO)_{10}]$ in solvents of varying properties. We show that, while certain properties of the solvent, such as hydrogen-bonding or the overlap of solvent and solute vibrational modes, can impact dynamics, and that polar solvents tend to favor symmetry breaking behavior, there are few broad trends that can be used to infer solvent–solute interactions. This necessitates the use of care when exchanging solvents for reacting systems or attempting to replace solvents with more sustainable alternatives.

EXPERIMENTAL

Sample preparation

$[Mn_2(CO)_{10}]$ (~1 mg, 2.56 μ mol) was dissolved in 600 μl of dry solvent (heptane, cyclohexane, THF, acetonitrile (MeCN), DMSO, isopropanol (^{i}PrOH), and methanol (MeOH)) to achieve a concentration of ~4 mM. All chemicals were purchased (Sigma Aldrich) and used as received.

IR spectroscopy

For IR spectroscopy measurements, a sample of each solution was placed in a standard transmission cell (Harrick) featuring two CaF_2 windows separated using a PTFE spacer of 50 μm thickness. These conditions produced a maximum absorbance of the ν_{CO} bands between 0.5 and 0.8 depending on the solvent. IR spectra were recorded at room temperature using a Bruker Vertex 70 spectrometer with a spectral resolution of 2 cm^{-1}.

The same $[Mn_2(CO)_{10}]$ samples were also used for the IR_{pump}–IR_{probe} and 2D-IR spectroscopy measurements. IR_{pump}–IR_{probe} experiments were performed using a regeneratively amplified Ti:sapphire laser system that produced mid-IR pulses via difference frequency mixing of the signal and idler beams generated using an optical parametric amplifier (OPA). The central frequency of the mid-IR pulses was selected to be resonant with the ν_{CO} modes of $[Mn_2(CO)_{10}]$ (~2011 cm^{-1}). The pulses had a bandwidth of 200 cm^{-1}, 100 fs pulse duration, and were produced with a repetition rate of 1 kHz. The output of the OPA was split using a CaF_2 beam splitter to give pump and probe pulse trains with an intensity ratio of 95:5. The two beams were overlapped spatially in the sample, and the pump–probe delay time was controlled via an optical delay line. After the sample, the probe beam was frequency dispersed using a spectrograph and detected using a 64 channel mercury cadmium telluride (MCT, HdCdTe) array detector giving a probe frequency resolution of 4.5–5 cm^{-1}. For data acquisition, the pump beam was chopped at 500 Hz to allow collection of $pump_{on}$–$pump_{off}$ difference spectra. The delay time was scanned from −5 to 800 ps. Spectra were recorded using ZZZZ, ZZYY (parallel and perpendicular), and magic angle (54.7°) polarization geometries. Vibrational relaxation dynamics were determined using both experimental data obtained using magic angle polarization and via calculation from data measured under ZZZZ and ZZYY conditions, which were found to show good agreement. Anisotropy decays were calculated from data measured under ZZZZ and ZZYY conditions.

The two-dimensional infrared (2D-IR) spectrometer incorporating twin, synchronized Yb-based amplified lasers has been described previously.[55] Mid-IR pulses with energies of 2.5 μJ, usable bandwidths of >200 cm^{-1}, and a pulse repetition rate of 50 kHz were directed into a 2DQuick spectrometer (PhaseTech). The spectrometer employed the pump–probe beam geometry for 2D-IR data collection.[50,56,57] A mid-IR pulse shaper generated and controlled the time delay (τ) between the pair of "pump" pulses, while an optical delay line controlled the waiting time (T_w) between the second pump and probe pulses. Signal measurement was achieved via twin 64-element HgCdTe array detectors configured to allow simultaneous collection of ZZZZ and ZZYY polarization-resolved data.

For a given value of T_w, τ was scanned in steps of 20 fs to a maximum delay time of 4 ps. A rotating frame frequency of 1585 cm^{-1} was applied. Each 2D-IR plot represents the average of 400 spectra, repeated three times, taking ~2 min to acquire.

RESULTS

IR absorption spectroscopy

The IR absorption spectra of $[Mn_2(CO)_{10}]$ in each of the solvents studied (Fig. 1) display three bands located close to 1980, 2010,

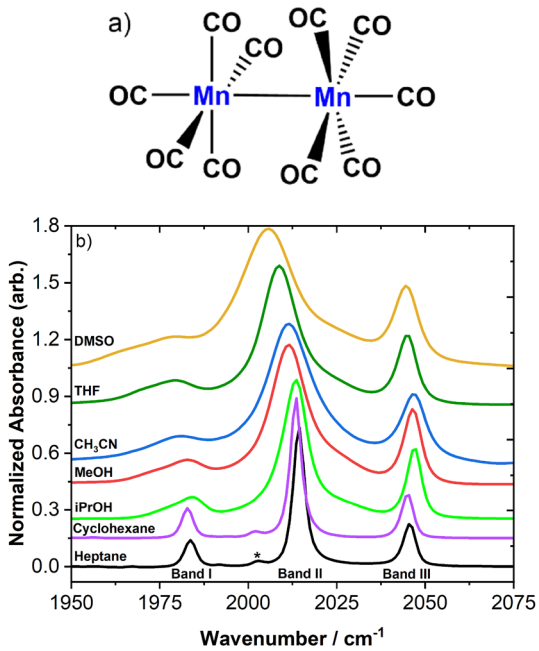

FIG. 1. (a) $[Mn_2(CO)_{10}]$ structure; (b) IR absorption spectra of $[Mn_2(CO)_{10}]$, in the solvents studied (ca 4 mM) following subtraction of the solvent spectrum. For ease of visibility, the absorbance of the central band in all solvents was scaled to the absorbance of the central band in ^{i}PrOH prior to applying a vertical offset.

and 2040 cm^{-1} (labeled I, II, and III, respectively), consistent with previous observations.[35,44,52,53,58] $[Mn_2(CO)_{10}]$ is a member of the D_{4d} point group, leading to assignment of the high and low frequency bands (I and III) to the B_2 symmetric and antisymmetric stretching modes of the axial carbonyls (ν_{CO}), respectively [Fig. 1(a) and Fig. S1]. These modes both have transition dipole moments that lie parallel to the metal–metal bond. The most intense, central band (II) is assigned to two degenerate E_1 modes that involve only motion of the equatorial carbonyls (Fig. S1). The transition dipole moments of these modes lie perpendicular to the metal–metal bond and to one another.[52,53,59] An additional low intensity peak near 2003 cm^{-1}, indicated by an asterisk in Fig. 1(b), was observed in the spectra of $[Mn_2(CO)_{10}]$ in heptane and cyclohexane solutions (Fig. 1, black and purple lines). This is attributed to the natural abundance of ^{13}C present in $[Mn_2(CO)_{10}]$.[52]

It is clear from Fig. 1(b) that changing the solvent has a number of consequences for the IR spectrum of $[Mn_2(CO)_{10}]$. The most obvious is a shifting of bands I and II to lower frequencies in comparison with the same band in heptane solution. By comparison, the position of band III is relatively unchanged by variation of the solvent.[60] These observations were quantified by fitting of the Gaussian line shapes to the spectra (Fig. S2 and Table S1). While a shift to lower wavenumbers for ν_{CO} bands might be expected in the presence of a protic solvent because hydrogen-bonding to a carbonyl reduces electron density in the C–O bond, it is the aprotic but more polar solvent, DMSO, which gives the greatest reduction in frequency.

Fitting of the spectra also allowed quantification of the response of the linewidth to the changing solvent. It was observed that the linewidth, quantified by the Full Width at Half Maximum (FWHM) parameter, of all the three IR active bands increased in all solvents relative to those in heptane and was found to be largest in DMSO. The measured FWHM values are in good agreement with previous reports.[34,52,61,62] Of particular note, a more pronounced line broadening with increasing solvent polarity was observed for band II relative to band I and particularly band III (Table I and Fig. S2). To investigate correlation with the solvent hydrogen bonding capabilities, FWHM was also plotted against Kamlet–Taft parameters (α and β); no obvious trend was observed (Fig. S3).

TABLE I. Polarity index values of the investigated solvents alongside the frequency position (cm^{-1}) and full width half maximum (FWHM, cm^{-1}) of bands II and III in IR absorption spectra determined by Gaussian fitting. Polarities are taken from Ref. 48.

Solvent	Polarity index	Frequency band II/band III (cm^{-1})	FWHM II/III (cm^{-1})
Heptane	0.1	2014/2045	4/4
Cyclohexane	0.2	2013/2045	4/4
^{i}PrOH	3.9	2013/2047	8/5
THF	4.0	2009/2045	11/6
MeOH	5.1	2011/2046	11/6
MeCN	5.8	2011/2047	12/8
DMSO	7.2	2006/2044	15/8

Previous reports have assigned this to band splitting and loss of degeneracy of the two E_1 modes arising from an energetic symmetry-breaking process.[34] The extent of splitting for each solvent was estimated by taking the difference between the determined FWHM of band II and band III [Fig. 2(a)]. This splitting was found to increase with solvent polarity, with no separation of the modes observed in heptane and cyclohexane.

In addition to changes in linewidth and frequency, the fitting process also revealed the appearance of new bands in the spectra of $[Mn_2(CO)_{10}]$ with increasing solvent polarity [*cf* spectra in heptane and MeOH in Figs. 2(b) and 2(c) and Fig. S2]. This can be ascribed to dynamic symmetry breaking causing previously IR inactive (Raman active) modes to gain oscillator strength.[52,53,59,63] Indeed, the positions of the new bands included in the fit correspond well to known Raman modes of $[Mn_2(CO)_{10}]$ (2024 cm^{-1} in hexane and 1972, 1979, 1998, 2021, and 2027 cm^{-1} for MeOH).[63,64]

IR_{PUMP}–IR_{PROBE} SPECTROSCOPY

Vibrational relaxation

IR_{pump}–IR_{probe} spectra of $[Mn_2(CO)_{10}]$ in heptane measured at a range of pump–probe time delays are shown in Fig. 3(a). Heptane solutions give rise to the narrowest linewidths, allowing assignment of the relevant features prior to discussion of the results obtained using other solvents (Fig. S4). Three negative peaks in the spectra are assigned to bleaches of the v = 0–1 transitions of the three ν_{CO} modes of $[Mn_2(CO)_{10}]$ identified in the IR absorption spectra. These peaks are labeled I–III in Fig. 3, consistent with the labeling in Fig. 1. A comparison of the bleaches with the (inverted) IR spectrum of $[Mn_2(CO)_{10}]$ in heptane (black) shows excellent agreement in terms

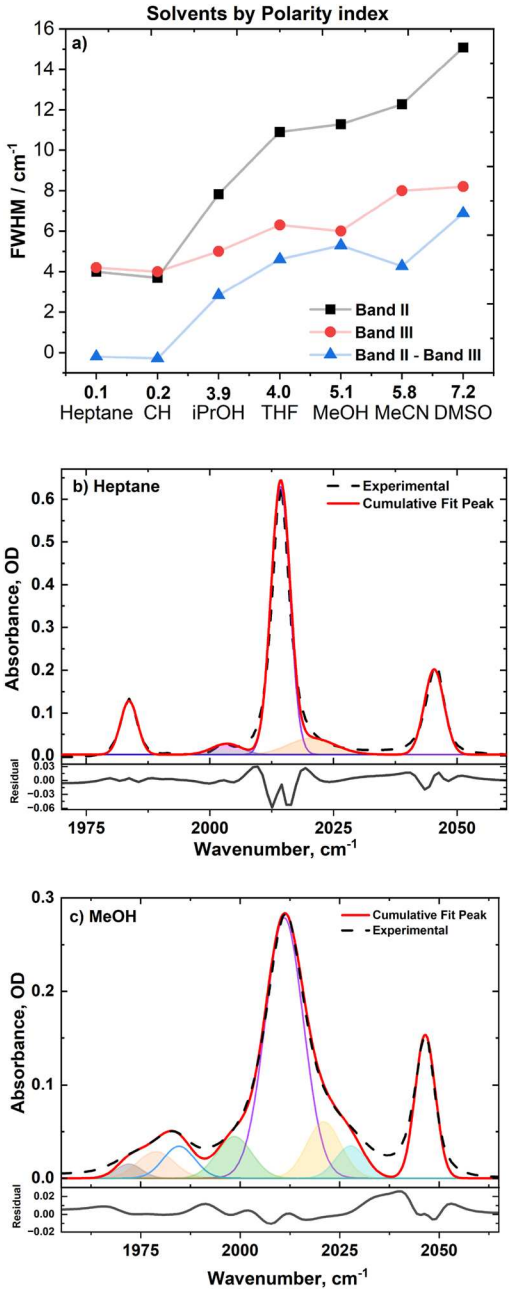

FIG. 2. (a) Variation in the FWHM determined by Gaussian fitting for band II (black squares) and band III (red circles) and the difference between them (blue triangles); the connecting lines function as guides to the eye; the points are equidistant not reflective of the polarity indices as displayed on the x axis. (b) and (c) Results of Gaussian fitting to the FTIR spectra of $[Mn_2(CO)_{10}]$ after solvent subtraction in (b) heptane and (c) MeOH. The dashed black lines correspond to experimental spectra, while the solid red lines are the resulting cumulative fit. The fit for heptane was achieved using five Gaussian line shapes corresponding to three IR active modes, the ^{13}C band (purple shaded band), and a Raman mode at 2024 cm^{-1} (orange). The fit for MeOH required the addition of further Raman modes (colored; see the text); hence, eight line shapes were employed. The residual plots at the bottom of the (b) and (c) graphs represent the accuracy of the fit to the data.

of frequency position and intensity ratio. In addition, a prominent positive peak was observed on the low wavenumber side of each of the three bleaches (labeled IV–VI). These peaks are assigned to transient absorptions involving the v = 1–2 transition of each of the three modes. The shift to lower wavenumbers is caused by the anharmonicity of the vibrational potential in each case, which is discussed in more detail in relation to 2D-IR data below. Also visible in Fig. 3(a) are additional, smaller positive peaks arising from transitions involving higher vibrationally excited states (e.g., v = 2–3). These are labeled V′ and VI′ in Fig. 3. The assignment is supported by fitting the IR_{pump}–IR_{probe} spectra to a set of Gaussian peaks using fixed anharmonic shifts (see Fig. S5).

The impact of changing the solvent on the appearance of IR_{pump}–IR_{probe} spectra is exemplified in Fig. 3(b), which shows the results obtained for a sample of $[Mn_2(CO)_{10}]$ in MeOH (see Fig. S4 for the remaining solvents). Once again, the inverted IR absorption spectrum is shown alongside the pump–probe data. The broadening of the three transitions I–III caused by MeOH, as revealed by IR absorption spectroscopy, leads to a number of changes to the pump–probe data relative to the heptane solution [Fig. 3(a)]. The positive and negative peaks in the pump–probe spectra are all broadened, causing the v = 0–1 bleaches and v = 1–2 transient absorptions (I–III and IV–VI, respectively) to dominate the spectra. The increase in linewidth also leads to overlap of peaks I and V with substantial loss in amplitude of the band I bleach, while peaks V′ and VI′ are no longer resolvable. In addition to the broadening of the bands, splitting of the E_1 transition and the gain in oscillator strength of the IR inactive modes in MeOH will also contribute to the overall shape of the spectrum, but these effects are hard to resolve individually. The impact of the new bands will be revisited in the discussion of 2D-IR spectra below. The effects observed in MeOH are repeated to varying degrees in the other solvents (see Fig. S4).

The peaks in the IR_{pump}–IR_{probe} spectra of the $[Mn_2(CO)_{10}]$ decay to the baseline as the pump–probe delay time increases because of vibrational relaxation (Fig. 3). In most cases, the observed relaxation dynamics were well-represented by a biexponential function (Fig. 4, Tables II and S2), revealing two distinct, fast and slow, timescales.[56] In contrast, the results from DMSO and cyclohexane solutions were both best described by a single exponential function. Due to complexities arising from band overlap, we focus our discussion on the bleach recovery timescale extracted from bands II and III.

In common with previous studies of vibrational relaxation,[28] we assign the fast component of the vibrational relaxation of $[Mn_2(CO)_{10}]$ to intramolecular vibrational energy redistribution (IVR) and the slow component to vibrational relaxation (T_1). The IVR timescale shows some solvent-dependence, spanning from 300 fs in CH_3CN to 1 ps in MeOH (Table II). Similarly, the vibrational relaxation time varies from 80 ± 1 ps (band III in MeOH) to 200 ± 4 ps (band III in heptane). The general trend in T_1 values follows the order heptane ≈ MeCN > cyclohexane > ^{i}PrOH > THF > DMSO ≈ MeOH. For a given solvent, the T_1 times also show some variation between bands. For example, the T_1 values obtained for band II in heptane and cyclohexane are ~40 ps shorter than those for band III, although the effect is less marked in other solvents with differences of less than 10 ps observed between the relaxation timescales of bands II and III for THF, MeOH, and DMSO.

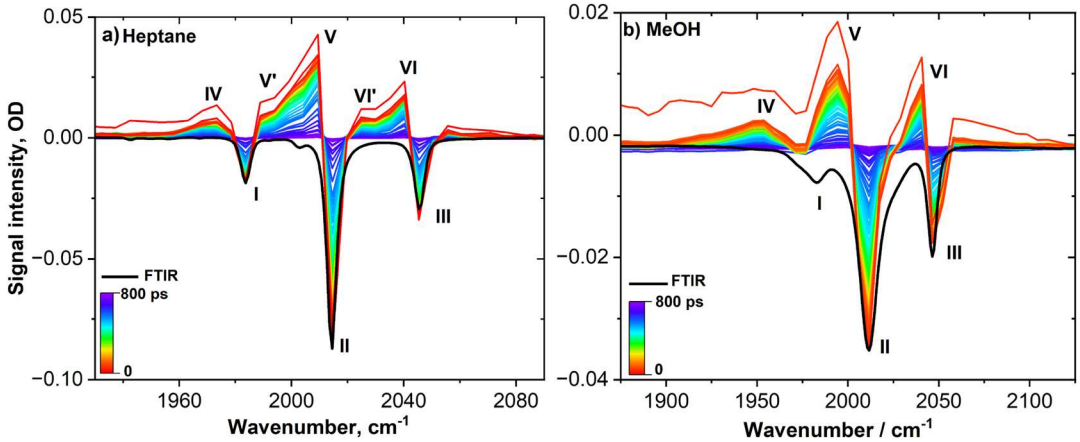

FIG. 3. IR_{pump}–IR_{probe} spectra of $[Mn_2(CO)_{10}]$ recorded under magic angle polarization conditions in (a) heptane and (b) MeOH at pump–probe delay times up to 800 ps. The bleaches (I, II, and III) correspond to the v = 0–1 transitions for each IR-active ν_{CO} vibrational mode, while the positive peaks (IV, V, and VI) correspond to the associated v = 1–2 transitions. The related FTIR spectra have been inverted and superimposed on the spectra (solid black lines). The magnitude of band II in the FTIR spectrum was scaled to match the intensity of bleach II.

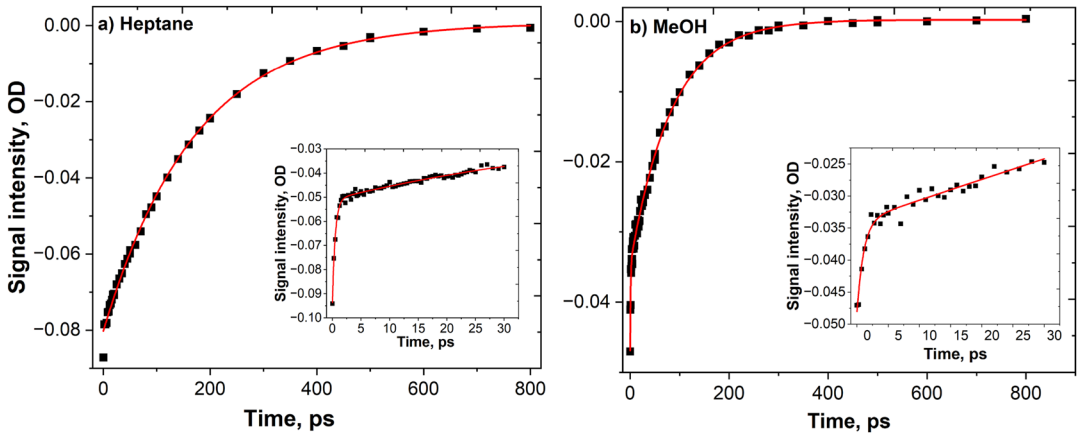

FIG. 4. Time dependence of the intensity of band II of $[Mn_2(CO)_{10}]$ in heptane (a) and MeOH (b), recorded under magic angle polarization conditions at pump–probe delay times up to 800 ps. The solid red lines show the result of a biexponential fit of the data. The insets show the time dependence of band II at pump–probe delay times up to 30 ps.

The IVR and T_1 timescales obtained for band II as a function of solvent are compared in Fig. 5. The horizontal axis of the graph is arranged in terms of increasing polarity index of the solvent. While there is a general tendency toward faster relaxation time (T_1) in more polar solvents, there are exceptions. For example, the T_1 values obtained for $[Mn_2(CO)_{10}]$ in MeCN are more comparable to those in heptane (band III: 197 vs 200 ps; band II: 184 vs 165 ps) than to more polar solvents. Similarly, the T_1 times of bands II and III in cyclohexane are ~50–60 ps shorter than in heptane despite both solvents being of similar physical properties. It is also noteworthy from Fig. 5 that the IVR and T_1 timescales appear to be broadly anticorrelated. While it is possible that this is an artifact of the fitting process, the large separation of the two timescales makes this unlikely. No correlation was observed when plotting the vibrational lifetimes vs Kamlet–Taft parameters, indicating that hydrogen bonding is not the only factor influencing vibrational energy dissipation, although it does have a contribution (see Fig. S3).

Anisotropy

The time dependence of the anisotropy parameter for band II of $[Mn_2(CO)_{10}]$ was obtained from IR_{pump}–IR_{probe} spectra using both ZZZZ and ZZYY polarization geometries. For all solvents, the decay of the anisotropy was found to be best represented by a mono-exponential function, producing a decay timescale of ~0.45–2 ps (Table II, Fig. S6). For non-degenerate bands with no appreciable fast IVR, the decay of anisotropy in the signal is generally due to

TABLE II. Vibrational dynamics of $[Mn_2(CO)_{10}]$ obtained from fitting IR_{pump}–IR_{probe} data to exponential functions. The solvents are listed in ascending order of the polarity index.[65] Quoted error bars are calculated as a standard error via the square root of reduced Chi-squared (Origin).

	IVR (ps)	Vibrational lifetime (T_1) (ps)		Anisotropy (ps)
Solvent	Band II	Band II	Band III	Band II
Heptane	0.50 ± 0.02	165 ± 2	200 ± 4	1.94 ± 0.14
Cyclohexane	⋯	104 ± 8	152 ± 13	1.50 ± 0.30
^{i}PrOH	0.56 ± 0.02	122 ± 2	133 ± 3	0.79 ± 0.03
THF	0.67 ± 0.03	113 ± 2	123 ± 8	0.58 ± 0.03
MeOH	0.98 ± 0.09	87 ± 1	80 ± 1	0.78 ± 0.06
CH_3CN	0.30 ± 0.05	184 ± 4	197 ± 5	0.47 ± 0.05
DMSO	⋯	85 ± 5	87 ± 3	0.42 ± 0.12

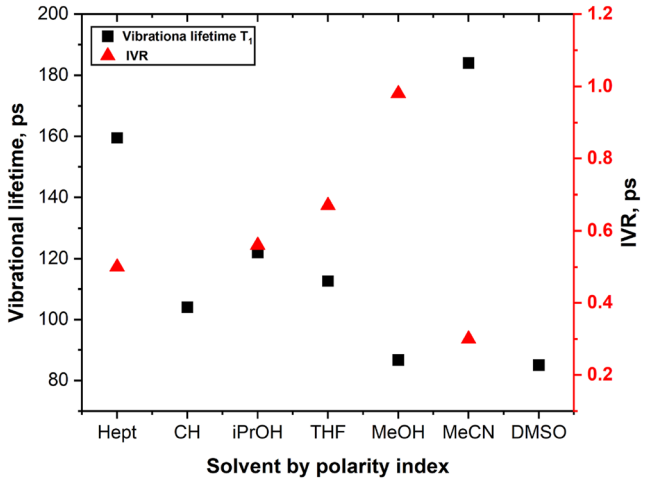

FIG. 5. IVR (red triangles) and T_1 (black squares) timescales measured for band II across all solvents. The solvents on the horizontal axis are ordered according to increasing polarity index. No fast component values are given for cyclohexane and DMSO, as the time dependencies of the intensities of the band II were found to be best represented by monoexponential functions.

rotational motion and thus correlates with properties such as solvent viscosity.[66–69] For degenerate bands, such as band II, or systems in which rapid IVR is present, these decays can also contain contributions from energy transfer processes.[63,66,70,71] The measured anisotropy decays in each solvent (Table II) reveal no correlation with solvent viscosity [see Fig. S7(a)]. Alongside the often subpicosecond magnitude of these values, this suggests that the values are unlikely to correspond to rotational motion of $[Mn_2(CO)_{10}]$. It also appears that as the degenerate E_1 modes become more separated, the anisotropy decays become faster [see Fig. S7(b)]. Finally, there is a striking similarity of the anisotropy decay timescales to the measured fast components of the vibrational relaxation, which were assigned to IVR [see Fig. S7(c)].[28] Of the solvents for which an IVR timescale could be extracted, only heptane, a non-polar solvent that gives no degenerate band splitting, shows no similarity between the anisotropy decay and the IVR timescale. In addition, examination of initial anisotropy (r0) values showed values ranging from 0.27 to 0.22 in the case of polar solvents consistent with partially scrambled dipoles. In the case of nonpolar solvents, the r0 value was 0.35. It thus seems appropriate to assign the anisotropy decay dynamics to the presence of fast IVR between the ν_{CO} modes.

2D-IR spectroscopy

2D-IR investigations were carried out in heptane, THF, and MeOH, representing apolar, polar aprotic, and polar protic environments, respectively. The 2D-IR spectrum of $[Mn_2(CO)_{10}]$ in heptane [Figs. 6(a) and 6(b)] displays a peak pattern consistent with three coupled modes, in line with previous studies. Negative peaks due to the fundamental transitions of the ν_{CO} modes appear along the spectrum diagonal, labeled I–III, consistent with the notation used above. Each diagonal peak is accompanied by a positive v = 1–2 peak, as identified in IR_{pump}–IR_{probe} spectra (IV–VI). The separations of these features in the 2D plot enabled diagonal anharmonicities of 11, 7, and 5 cm^{-1} to be measured for modes I, II, and III, respectively, which are consistent with those extracted from Gaussian fitting of the IR_{pump}–IR_{probe} data (see Fig. S5). We note that some anharmonicities differ slightly from previously reported values,[53] possibly arising from the use of fully-absorptive spectra in this case rather than an absolute value representation. Six off-diagonal features are also evident in the 2D-IR spectra of $[Mn_2(CO)_{10}]$ in heptane, indicating the mutual vibrational coupling of the ν_{CO} modes. These features consist of negative peaks (1–6) arising from the fundamental transitions of the coupled mode and positive peaks arising from transitions to the combination state of the pair of coupled modes (1′–6′).[50] Mixed mode (or off-diagonal) anharmonicities, obtained by measuring the probe frequency separation of the n and n′ components (for n = 1–6), provide a measure of the strength of the coupling and were found to be on the order of 6–9 cm^{-1}.[53]

In addition to these peaks, which are expected for a set of three coupled modes, extra features appear in the 2D-IR spectrum of $[Mn_2(CO)_{10}]$ in heptane at short values of T_w. In the ZZZZ polarization spectrum, an extra diagonal peak at a frequency of ~2000 cm^{-1} was identified [indicated by the pink circle in Fig. 6(a)]. This peak might be assigned to modes of $Mn_2(CO)_{10}$ involving

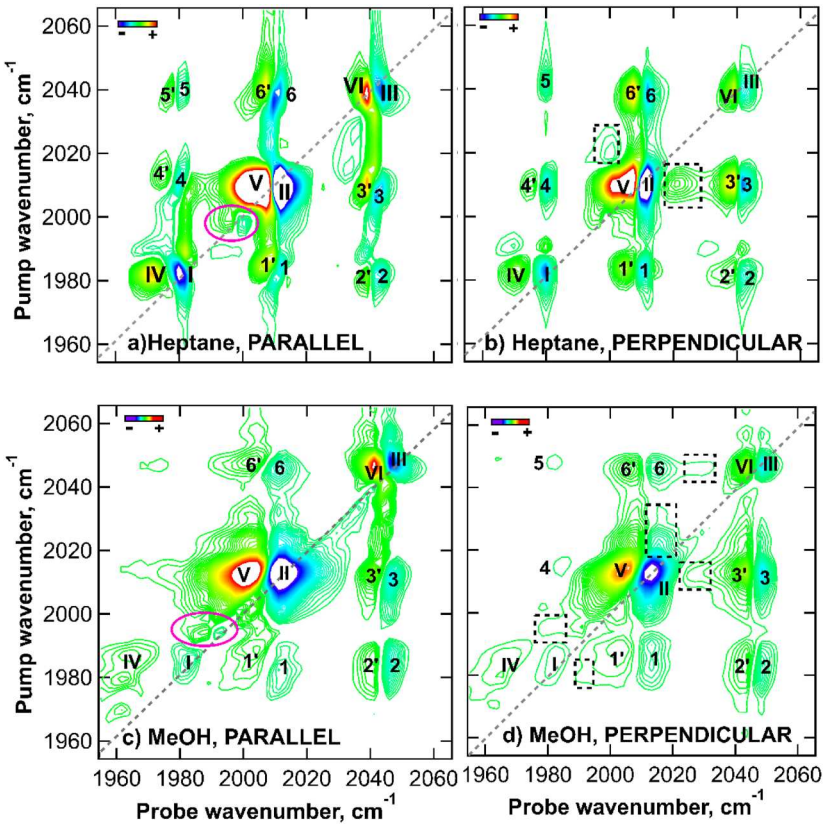

FIG. 6. 2D-IR spectra of $[Mn_2(CO)_{10}]$ with T_w = 0 fs in heptane (a) and (b) and MeOH (c) and (d), obtained under ZZZZ (parallel) and ZZYY (perpendicular) polarization conditions. Note: the equivalent spectra obtained with T_w = 500 fs show an identical form to those obtained with T_w = 0 fs, confirming that the data are not affected by pump–probe overlap effects (see Figs. S9 and S11).

the naturally abundant ^{13}CO ligands observed in the FTIR spectrum. However, a Raman mode of the compound is also reported at 1997 cm^{-1} (see Fig. S8 for an overlay of the simulated FTIR spectrum and the corresponding 2D-IR plot). In the ZZYY polarization spectrum, off-diagonal peaks were observed near (pump, probe) = (2020, 2000 cm^{-1}) and (2010, 2020 cm^{-1}) [Fig. 6(b), black dashed line boxes]. In the former case, the two frequencies do not match IR active modes of $[Mn_2(CO)_{10}]$ but lie close to Raman modes, while in the latter case, the pump frequency matches band II, but the probe frequency aligns well with a Raman-active mode. We thus assign these to the product of coupling between normally dark Raman active modes and coupling between IR and Raman-active modes.

Considering the evolution of the 2D-IR spectrum of $[Mn_2(CO)_{10}]$ in heptane with T_w, the 2D line shapes were analyzed to investigate the presence of inhomogeneous broadening and spectral diffusion. The spectra in Fig. 6 show that, based on the 2D line shape, there is little inhomogeneous broadening present for $[Mn_2(CO)_{10}]$ in heptane (diagonal to antidiagonal ratio = 0.84 at T_w = 500 fs) and that the peak shape undergoes little evolution to a T_w of 100 ps (see Fig. S9). CLS and IvCLS methods were also used to confirm these conclusions (see Fig. S10).[72] This observation is consistent with previous reports showing that the ν_{CO} line shapes of the compound are not strongly influenced by solvent motion, although picosecond-timescale dynamics were extracted by use of the inhomogeneity index.[34] Inspection of the τ-dependence of the 2D-IR signals arising from the $Mn_2(CO)_{10}$ v = 0–1 bands indicates a coherence decay of 3.3 ps; this implies a homogeneous linewidth of 3.2 cm^{-1}. Given that the FWHM of the equivalent bands in the IR absorption spectrum for heptane (Table I) is 4 cm^{-1}, we conclude that the lines are largely homogeneously broadened.

Finally, inspection of the spectra at longer values of T_w > 2 ps showed the appearance of new peaks arising from the IVR process (See Fig. S9). These arise as a consequence of vibrational energy redistribution from the pumped mode to the v = 1 levels of other modes such that the probe pulse can excite the v = 1–2 transition of the indirectly populated state. These peaks and their arrival dynamics are consistent with data collected using IR_{pump}–IR_{probe} methods.

The 2D-IR spectrum of $[Mn_2(CO)_{10}]$ in MeOH [Figs. 6(c) and 6(d)] contains a comparable set of peaks to those in heptane. It is clear from the spectra that, although the lines in the FTIR and IR_{pump}–IR_{probe} spectra exhibited broadening (Figs. 1 and 3), this does not appear to manifest as inhomogeneous broadening in the 2D-IR spectrum. The coherence decay of 1 ps observed in this case implies a greater homogeneous linewidth for the carbonyl bands of $[Mn_2(CO)_{10}]$ in polar solvents of 10.2 cm^{-1}. These appear to be consistent with the FWHM of 11 cm^{-1} obtained from the FTIR absorption spectra. Similarly to heptane, spectral diffusion is not evident in these spectra, with the diagonal peaks retaining the same line shape from the earliest T_w (also verified by CLS and IvCLS methods). Another consequence of the line broadening is that the set of

off-diagonal peaks to mode I above the diagonal (labeled 4, 5 in Fig. 6(a) are undetected, which is assumed to be due to overlap and cancellation between positive and negative features, as mentioned above. However, the equivalent features below the diagonal are present, confirming that the coupling is retained in MeOH. Indeed, the mixed mode anharmonicities of the ν_{CO} modes of $[Mn_2(CO)_{10}]$ are unchanged in MeOH as compared to heptane. By contrast, the single mode anharmonicities show some sensitivity to the solvent with values for modes I–III in MeOH of 18, 11, and 6 cm^{-1} compared to 11, 7, and 5 cm^{-1} in heptane. 2D-IR spectra obtained for THF solutions were very similar to those in MeOH (see Figs. S11 and S12), with on diagonal anharmonicities measured to be 14, 10, and 5 cm^{-1} for modes I–III, respectively.

As observed in heptane, additional peaks, not consistent with the IR-active modes of $[Mn_2(CO)_{10}]$, appear in the 2D-IR spectra obtained in polar solvents. In the case of the MeOH solution, these additional features also occur both on and off the diagonal [pink circles in Fig. 6(c) and black squares in Fig. 6(d)] and correspond to Raman active modes for $[Mn_2(CO)_{10}]$ in MeOH that are reported in the literature (1972, 1979, 1998, 2021, and 2027 cm^{-1}; see Fig. S8 for an overlay of the simulated FTIR, including Raman bands and the corresponding 2D-IR plot).[63,64]

DISCUSSION

The data presented reveal a solvent dependency on the behavior of $[Mn_2(CO)_{10}]$, which can be broadly separated into two areas: an impact on the spectroscopy, symmetry, and mode structure of $[Mn_2(CO)_{10}]$ and modulation of the observed vibrational relaxation dynamics of the ν_{CO} modes.

Effect of the solvent on molecular symmetry

The IR absorption data for $[Mn_2(CO)_{10}]$ show changes in band frequencies and linewidths upon moving from non-polar to polar solvents. The most striking changes, however, are exhibited by band II, which is assigned to a pair of E_1 symmetry modes. While the FWHM of band III (B_2 symmetry) was observed to double on moving from the heptane solution to DMSO, from the solvent with the lowest polarity index to the most polar solvent, band II increases in width by almost a factor of four. Examining the trend in FWHM values (Table I) shows that the difference between the width of band II and band III increases in a manner that correlates with solvent polarity.

A common cause of increased linewidths in strongly-interacting solvents is inhomogeneous broadening. However, the 2D-IR spectra do not show evidence of peak elongation along the diagonal. This is even the case in the solvents likely to make hydrogen-bonds with the CO ligands of $[Mn_2(CO)_{10}]$ (MeOH and ^{i}PrOH). While somewhat surprising, this is consistent with previous studies of $[Mn_2(CO)_{10}]$ in a range of linear alcohol solvents.[52] The inhomogeneous contribution to the spectral linewidth was found to be small with little evidence of strong changes in the 2D peak shape, as we see here. In the previous study the authors exploited the inhomogeneity index to extract spectral diffusion times for $[Mn_2(CO)_{10}]$ modes, observing few picosecond spectral diffusion timescales. The indication, therefore, is that, while sensitive to environmental effects, the ν_{CO} modes of the compound are not interacting strongly with the solvents to the extent that significant inhomogeneous broadening is observable.

This leads to the conclusion that the increase in width of the E_1 band (II) is due to other factors. One possibility is that the more polar solvents are removing the degeneracy of the two E_1 components, leading to splitting of band II, which would not be mirrored in bands I and III. This cannot be confirmed from the IR absorption data where two components of peak II cannot be resolved. In the case of the 2D-IR data, some indication of a second component to the diagonal peak II is visible at short values of T_w [Fig. 6(c)], although the separation is not sufficient to allow unambiguous identification of two separate peaks or the presence of the expected off-diagonal peaks linking them. Similarly, the antidiagonal slice method failed to show any splitting of the fundamental mode or cross peaks (Fig. S13).[73,74] In addition to MeOH, it is clear that the other polar solvents DMSO, MeCN, and THF and the protic solvent ^{i}PrOH all cause broadening of the E_1 pair of modes, suggesting that a similar effect is taking place in all of the non-hydrocarbon solvents.

It is relevant to this discussion that extra peaks appear in the 2D-IR spectrum of $[Mn_2(CO)_{10}]$, especially in the more polar solvents, at frequencies matching those reported for Raman modes. This implies that the formally IR-inactive bands have become partially allowed, an effect that would also require a change in symmetry from the formal D_{4d} structure assigned to $[Mn_2(CO)_{10}]$. Even in heptane, where most of the Raman modes remain dark, cross peaks to them are visible, suggesting that the effect may be present to a much smaller degree even in non-polar solvents.

A further indication of symmetry breaking in the solvents studied here arises from anisotropy data. Analysis of the bleach of band II produced monoexponential anisotropy decays across all solvents on timescales of ~0.4–2 ps (Table II). Anisotropy decays typically report on the rotation of the direction of the transition dipole moment of the vibrational mode being studied.[66,68,69,75–78] As such, reported anisotropy decays typically correlate with solvent viscosity or other properties, such as hydrogen bonding.[63,66,75,78,79] For band II, no correlation was identified between the anisotropy decays and solvent viscosities, and in all solvents but heptane, the anisotropy decay was assigned to IVR based on similarity of timescale. In this context, the observed generally opposing trends in the anisotropy decay timescale and the FWHM difference between bands II and III, which relates to E_1 band splitting [Fig. S7(b)], are interesting. Considering that, under normal circumstances, the transition dipole moments of the two E_1 modes are directed perpendicular to each other, it is possible that, as the symmetry of $[Mn_2(CO)_{10}]$ is broken, the directions of the transition dipole moments become non-orthogonal. This might be expected to result in anisotropy decay times becoming shorter in more polar solvents.

The observation of symmetry-breaking effects in a range of solvents shows the ability of the environment to influence the nature of the vibrational potential energy surfaces of $[Mn_2(CO)_{10}]$. The mechanism by which this happens has two possible origins. One involves symmetry breaking arising from solvent coordination or similar interactions that induce a distortion of the molecular geometry. Indeed, the extent of symmetry breaking reflects the degree of band shifting and broadening, consistent with increased solute–solvent interactions. However, a second more preferable possibility, also

proposed elsewhere, is a "dynamical" symmetry effect.[35,52] Through Molecular Dynamics (MD) simulations of $[Mn_2(CO)_{10}]$ in a series of linear alcohols, it was suggested that a more fluxional solvation environment disrupts the delocalization across the carbonyl vibrational modes and the coupling between them, inducing an "energetic symmetry breaking."[52] While the results obtained here are not directly comparable as the authors focused purely on a hydrogen-bonding environment, the lack of obvious inhomogeneous broadening would tend to support a situation where there is no strong direct interaction with $[Mn_2(CO)_{10}]$ by the solvents. Our data also show that the symmetry-breaking mechanism is present in polar as well as protic solvents and to a lesser extent in non-polar solvents. This implies that interactions between $[Mn_2(CO)_{10}]$ and the solvent, whether apolar, polar, or protic, lead to the Gaussian disorder proposed in vibrational aggregate models, so that the degree of increase in the observed linewidth is moderate but exacerbates the effects associated with loss of symmetry.

Effect of the solvent on vibrational relaxation

Analysis of the dynamics of $[Mn_2(CO)_{10}]$ in the different solvents produced two distinct timescales: a slow component on the order of hundreds of picoseconds, assigned to IVR, and a fast component on the order of hundreds of femtoseconds, assigned to vibrational relaxation (Fig. 5, Table II).

IVR dynamics

The fast relaxation component was assigned to IVR, where energy balance is ensured by transfer of energy to or from the solvent.[80,81] IVR has been widely reported for many metal carbonyl systems and is typically observed on the order of a few picoseconds.[30,31,36,42,75,82,83] The times found here are somewhat fast (~0.3–1 ps), but they are in good agreement with a previous report of ~600 fs for $[Mn_2(CO)_{10}]$ in cyclohexane,[28] and subpicosecond IVR times have been quoted elsewhere.[84,85] Other reports of IVR for $[Mn_2(CO)_{10}]$ have been longer, with times of ~3 ps in cyclohexane and ~2–8 ps in a series of linear alcohols.[35,53] However, those values were obtained by 2D-IR spectroscopy and, therefore, represent the intramolecular transfer of energy between two selected vibrational modes rather than the broadband picture generated by IR pump–probe experiments.

IVR can be affected by a multitude of solute and solvent specific properties, such as internal degrees of freedom, coupling between vibrational modes, the energy gap between them, solute–solvent interactions (e.g., hydrogen-bonding), and the low frequency density of states of the solvent.[31,66,81] The particularly fast IVR times observed for $[Mn_2(CO)_{10}]$ here could be the result of solute specific factors—the complex contains 10 highly delocalized carbonyl groups, and the vibrational modes are strongly coupled with relatively small energy gaps between them (~31 cm^{-1} in heptane).[52] In the IR absorption spectra, the bands become increasingly broad and are shifted to lower wavenumbers in more polar solvents, implying stronger solute–solvent interactions. In some cases, this has been reported to assist IVR, resulting in faster rates.[86,87] No such correlation is observed here, with IVR, instead, becoming slower in more polar solvents, except for MeCN, which produces the fastest time (0.30 ± 0.05 ps). In fact, a hydrogen-bonding-induced hindrance of IVR was identified previously for $[Mn_2(CO)_{10}]$ in a series of linear alcohols, whereby the IVR timescale became longer with increasing number of hydrogen-bonds to the solute.[52] Indeed, in this study, MeOH produced the longest IVR time (0.98 ± 0.09 ps).

It is also valuable to consider the low frequency density of states offered by the solvent at the energy difference between coupled vibrational modes undergoing IVR. It is these low frequency modes of the solvent that can ensure energy conservation by compensating for the energy mismatch between the modes.[31,88] Therefore, the greater the density of states of the solvent at the value of energy mismatch, the faster the intramolecular energy process.[31] Optical Kerr Effect (OKE) spectroscopy can be used to provide a measure of these low frequency density of states through the Reduced Spectral Density (RSD).[89] For the solvents studied here, a maximum of spectral density was reported at ~25 to ~50 cm^{-1} in heptane, MeOH, THF, and MeCN.[89–91] As the separation between bands I and II and bands II and III across all solvents is ~25–35 cm^{-1}, this would seem to be the most likely mechanism. Indeed, the RSD amplitude of MeCN is significantly larger than both MeOH and heptane (THF amplitudes not given),[90] consistent with the comparatively rapid IVR observed in MeCN.

Vibrational relaxation

The slow relaxation component has been attributed to vibrational relaxation to the ground state, and the timescales observed are consistent with previous studies.[28,33,36,42,52,53,70,92] Several solute and solvent specific properties can affect the vibrational lifetime;[66,78,80,93–96] hydrogen-bonding of the solvent to a carbonyl ligand of a metal complex, for example, is known to shorten the lifetime.[36,78,80,85,93,94] In this study, shorter lifetimes were indeed observed for the protic solvents, with ^{i}PrOH giving shorter lifetimes than both heptane and cyclohexane and MeOH giving the shortest time overall (Table II). While it is also possible to assign this to increasing polarity, MeCN, which is more polar than both protic solvents, produces lifetimes comparable to heptane. This implies that hydrogen-bonding is a key factor in the acceleration of vibrational relaxation. Also noteworthy is that THF and DMSO, both aprotic solvents, produced lifetimes comparable to ^{i}PrOH and MeOH. Upon examination of the IR absorption spectra of THF and DMSO, bands resonant with the modes of $[Mn_2(CO)_{10}]$ were found (Fig. 7), suggesting that these resonant modes may be acting as additional pathways for vibrational energy dissipation. Such a mechanism has been identified previously in a study of CORM-2 $[RuCl_2(CO)_3]_2$ in H_2O.[36]

The observed trend in the vibrational lifetime of $[Mn_2(CO)_{10}]$ across the range of solvents studied here can therefore be rationalized as relating broadly to solvent polarity, augmented in some cases by solvent hydrogen bonding (^{i}PrOH and MeOH) and the presence of resonant modes (THF, MeOH, DMSO, and cyclohexane). In the case of the overlap of solvent modes, this can be a surprisingly effective process, as evidenced by the acceleration of relaxation in cyclohexane vs heptane [Fig. 7(a)], despite the overlap arising only from a relatively weak overtone or combination band with band I of the compound. Moreover, given that THF, an aprotic solvent with a resonant band, produces lifetimes shorter than ^{i}PrOH, a protic solvent with no resonant bands (~120 vs ~140 ps), it could be concluded that resonant solvent bands are a more dominant intermolecular relaxation pathway than hydrogen bonding. Similarly, MeOH and

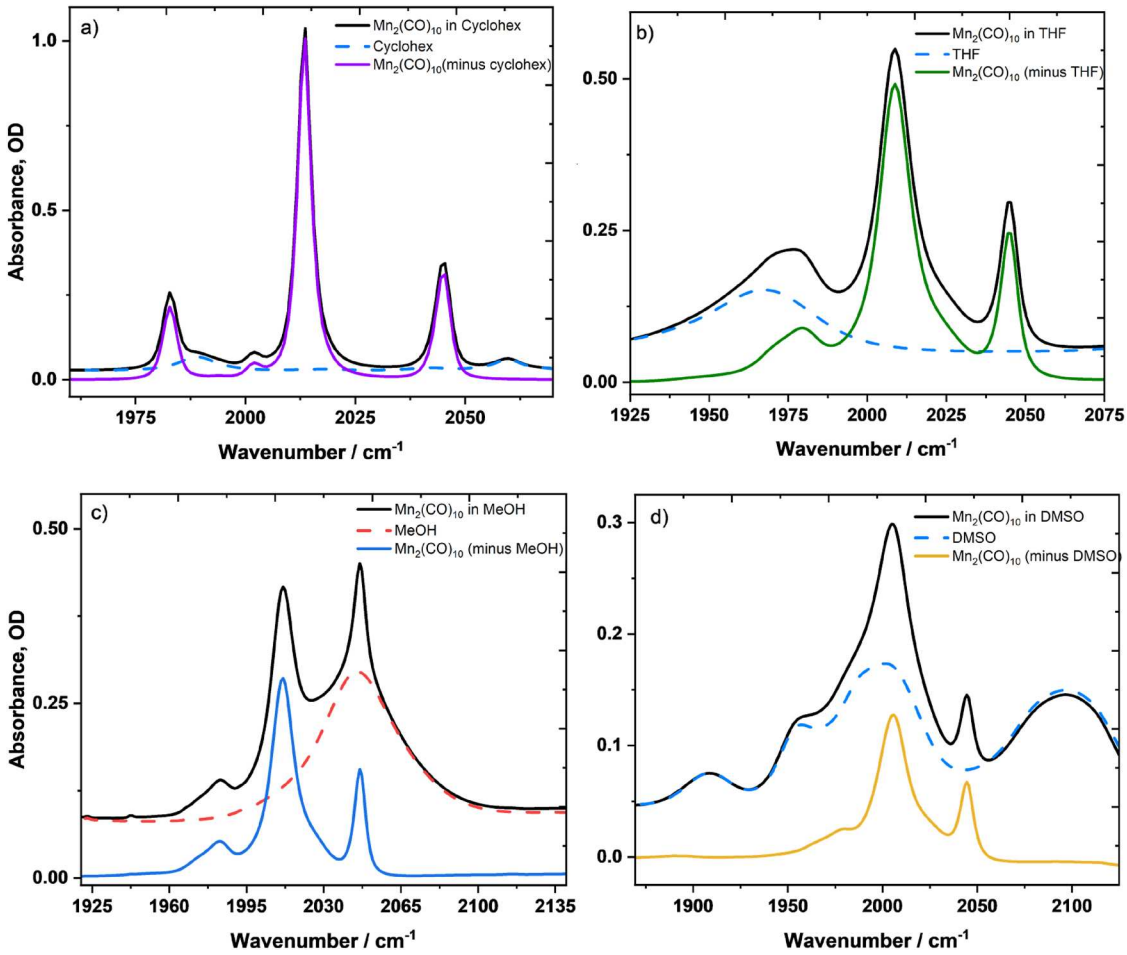

FIG. 7. FTIR spectra of $[Mn_2(CO)_{10}]$ in (a) cyclohexane, (b) THF, (c) MeOH, and (d) DMSO before and after solvent subtraction; the FTIR spectrum of the solvent is given by the dashed line in each of the panels.

DMSO produce comparable lifetimes (~80–90 ps), yet MeOH is protic and possesses a band resonant with one IR active mode of the complex, while DMSO is aprotic but has extensive overlap will all four IR active modes. The numerous IR bands of DMSO available to accept energy from $[Mn_2(CO)_{10}]$ may therefore assist vibrational relaxation to the same extent as the combined effect of hydrogen bonding and a single resonant band in MeOH.

In non-polar solvents (e.g., heptane, cyclohexane), bands showed a different relaxation rate. It is plausible that this may be caused by the lack of line broadening in these solvents, whereas in the more polar solvents, the measurement of relaxation is affected due to band overlap and cancellation. It is also possible that, with the longer timescales observed in polar solvents, the differences between the relaxation dynamics of individual modes become more apparent. As mentioned above, the presence of solvent-dependent relaxation is indicative of each mode interacting differently with the solvent; however, there seems to be no simple relationship between solvent properties and relaxation dynamics.

It is interesting to note that the vibrational lifetime and IVR timescales observed for $[Mn_2(CO)_{10}]$ in the solvents studied display approximately opposing trends. This suggests that intermolecular vibrational energy dissipation to the solvent can be accelerated at the expense of IVR or vice versa. It is not clear that the two mechanisms are necessarily linked; however, for example, while hydrogen-bonds can inhibit IVR, hydrogen-bonds and overlapping solvent modes can accelerate relaxation, but each occurs through discrete mechanisms rather than being necessarily competitive.

Previously reported IR_{pump}–IR_{probe} anisotropy experiments on $[Mn_2(CO)_{10}]$ in cyclohexane indicated a biexponential decay for bleach II with a fast component of ~600 fs assigned to IVR and a slow component of 15.8 ± 3.5 ps assigned to orientational relaxation.[28] The fast ~600 fs is of a similar magnitude to the decays measured here, but a slower component was not observed. Even when attempting to fit the data to a biexponential function, which was not possible in most cases, the slower component was measured

on the order of 1–2 ps. If a pure rotational motion could be resolved, such as that of the entire molecule, a value on the order of tens of picoseconds would indeed be expected given the volume of $[Mn_2(CO)_{10}]$ [1346.9(5) Å^3]. To test that the anisotropy decays observed here did not arise from some experimental error, a control experiment was performed by measuring the anisotropy decay of $W(CO)_6$ in heptane. Using the same experimental conditions and method of obtaining the decays as before, a time of 5.5 ± 0.2 ps was measured, which is in good agreement with a time of 4.7 ± 0.5 ps reported elsewhere.[75]

CONCLUSION

The vibrational dynamics of $[Mn_2(CO)_{10}]$ have been investigated in various solvation environments using IR absorption, IR_{pump}–IR_{probe}, and 2D-IR spectroscopy. The results reveal band shifting and broadening, potential loss of E_1 mode degeneracy, and the appearance of new bands, especially in the more polar solvents, commensurate with a solvation environment that induces symmetry breaking of the complex. Coupled with a lack of strong inhomogeneous broadening-related effects on the 2D line shapes, we believe that this is in agreement with previous suggestions of a vibrational-aggregate type model for $[Mn_2(CO)_{10}]$, and this data extend the analysis to a broad range of solvents and solvent types.

Time-resolved studies revealed two solvent dependent vibrational relaxation pathways—relaxation back to the ground state (vibrational lifetime, ~80–250 ps) and rapid IVR (~0.3–1 ps). The trends observed highlight a complex scenario where, rather than each individual solvent property producing a predictable effect, they were found to act collectively and to different extents depending upon the specific solvation environment. Despite this, it was possible to identify effects due to hydrogen-bonding and the presence of resonance between IR bands of the solvent and solute, which led to a shortening of the vibrational lifetime. IVR exhibited an opposing trend, showing the complex interplay between intermolecular and intramolecular relaxation routes, where hydrogen-bonding to the solvent hindered the rate of IVR, while the low frequency density of states of the solvent at the values of energy mismatch between the coupled vibrational modes would facilitate energy transfer, particularly in the case of MeCN.

Overall, these results emphasize the importance of the solvation environment in consideration of the reaction mechanism and highlight its potentially multivariate behavior. They also offer insights into the dynamics of $[Mn_2(CO)_{10}]$ specifically, but the lessons are likely to be broadly applicable. An open question is the way in which these solvent factors relate to or control the photochemistry and dynamics of the subsequent catalytic reactions. In photochemical reactions, it is proposed that $[Mn_2(CO)_{10}]$ dissociates to form $[Mn(CO)_5]$, which is then responsible for the subsequent chemistry. However, when $[Mn_2(CO)_{10}]$ acts under thermal conditions[27] through CO-loss, the nature of the catalyst-solvent interactions will have a direct effect on the potential activation pathways. Our results do, however, point to the likely necessity of considering and measuring specific solvent factors when choosing alternative or new solvents for a chemical process.

SUPPLEMENTARY MATERIAL

See the supplementary material for the complete set of FTIR, pump–probe, and 2DIR measurements in the various solvents; Gaussian fitting of the IR spectra; and the full set of vibrational relaxation decays.

ACKNOWLEDGMENTS

J.M.L., I.J.S.F., and N.T.H. acknowledge the funding from EPSRC (Grant No. EP/W031914/1). N.T.H., I.J.S.F., and S.G. acknowledge support from EPSRC (Grant No. EP/W021404/1), while B.P. acknowledges funding from the Leverhulme Trust (Grant No. RPG-2021-160). J.M.L. and I.J.S.F. were supported by Royal Society Industry Fellowships (Grant Nos. INF\R1\221057 and INF\R2\202122, respectively). A.L.F. acknowledges the PhD studentship funding from STFC and the University of York.

AUTHOR DECLARATIONS

Conflict of Interest

The authors have no conflicts to disclose.

Author Contributions

Amy L. Farmer: Data curation (lead); Formal analysis (equal); Investigation (equal); Writing – original draft (equal). **Barbara Procacci**: Conceptualization (equal); Data curation (equal); Formal analysis (equal); Investigation (equal); Methodology (equal); Supervision (equal); Writing – original draft (equal). **Daniel J. Shaw**: Methodology (supporting); Writing – original draft (supporting). **Sabina Gurung**: Methodology (supporting); Writing – original draft (supporting). **Ian J. S. Fairlamb**: Funding acquisition (equal); Writing – original draft (supporting). **Jason M. Lynam**: Data curation (supporting); Funding acquisition (equal); Project administration (equal); Supervision (supporting); Writing – original draft (supporting). **Neil T. Hunt**: Conceptualization (equal); Formal analysis (equal); Funding acquisition (equal); Project administration (equal); Supervision (equal); Validation (equal); Writing – original draft (equal).

DATA AVAILABILITY

The data that support the findings of this study are available within the article and its supplementary material.

REFERENCES

[1] M. Moselage, J. Li, and L. Ackermann, ACS Catal. **6**, 498 (2016).
[2] G. Pototschnig, N. Maulide, and M. Schnürch, Chem. - Eur. J. **23**, 9206 (2017).
[3] B. Su, Z. C. Cao, and Z. J. Shi, Acc. Chem. Res. **48**, 886 (2015).
[4] L. A. Hammarback, J. B. Eastwood, T. J. Burden, C. J. Pearce, I. P. Clark, M. Towrie, A. Robinson, I. J. S. Fairlamb, and J. M. Lynam, Chem. Sci. **13**, 9902 (2022).
[5] L. A. Hammarback, A. Robinson, J. M. Lynam, and I. J. S. Fairlamb, J. Am. Chem. Soc. **141**, 2316 (2019).

[6]N. P. Yahaya, K. M. Appleby, M. Teh, C. Wagner, E. Troschke, J. T. W. Bray, S. B. Duckett, L. A. Hammarback, J. S. Ward, J. Milani, N. E. Pridmore, A. C. Whitwood, J. M. Lynam, and I. J. S. Fairlamb, Angew. Chem. **128**, 12643 (2016).
[7]M. Ciftci, M. A. Tasdelen, and Y. Yagci, Polym. Chem. **5**, 600 (2014).
[8]M. Ciftci, M. A. Tasdelen, and Y. Yagci, Polym. Int. **65**, 1001 (2016).
[9]J. Dong, X. Wang, Z. Wang, H. Song, Y. Liu, and Q. Wang, Chem. Commun. **55**, 11707 (2019).
[10]N. Huther, P. T. McGrail, and A. F. Parsons, Eur. J. Org Chem. **2004**, 1740.
[11]Y. X. Ji, L. J. Wang, W. S. Guo, Q. Bi, and B. Zhang, Adv. Synth. Catal. **362**, 1131 (2020).
[12]P. Nuhant, M. S. Oderinde, J. Genovino, A. Juneau, Y. Gagné, C. Allais, G. M. Chinigo, C. Choi, N. W. Sach, L. Bernier, Y. M. Fobian, M. W. Bundesmann, B. Khunte, M. Frenette, and O. O. Fadeyi, Angew. Chem. **129**, 15511 (2017).
[13]J. D. Firth, L. A. Hammarback, T. J. Burden, J. B. Eastwood, J. R. Donald, C. S. Horbaczewskyj, M. T. McRobie, A. Tramaseur, I. P. Clark, M. Towrie, A. Robinson, J. P. Krieger, J. M. Lynam, and I. J. S. Fairlamb, Chem. - Eur. J. **27**, 3979 (2021).
[14]L. Wang, J. M. Lear, S. M. Rafferty, S. C. Fosu, and D. A. Nagib, Science **362**, 225 (2018).
[15]W. Liu, D. Zell, M. John, and L. Ackermann, Angew. Chem., Int. Ed. **54**, 4092 (2015).
[16]S. Sueki, Z. Wang, and Y. Kuninobu, Org. Lett. **18**, 304 (2016).
[17]X. Yang, X. Jin, and C. Wang, Adv. Synth. Catal. **358**, 2436 (2016).
[18]S. H. Cai, L. Ye, D. X. Wang, Y. Q. Wang, L. J. Lai, C. Zhu, C. Feng, and T. P. Loh, Chem. Commun. **53**, 8731 (2017).
[19]S. L. Liu, Y. Li, J. R. Guo, G. C. Yang, X. H. Li, J. F. Gong, and M. P. Song, Org. Lett. **19**, 4042 (2017).
[20]Y. F. Liang, L. Massignan, and L. Ackermann, ChemCatChem **10**, 2768 (2018).
[21]Y. Kuninobu, Y. Nishina, T. Takeuchi, and K. Takai, Angew. Chem., Int. Ed. **46**, 6518 (2007).
[22]R. He, X. Jin, H. Chen, Z. T. Huang, Q. Y. Zheng, and C. Wang, J. Am. Chem. Soc. **136**, 6558 (2014).
[23]W. Liu, J. Bang, Y. Zhang, and L. Ackermann, Angew. Chem., Int. Ed. **54**, 14137 (2015).
[24]W. Liu, S. C. Richter, Y. Zhang, and L. Ackermann, Angew. Chem., Int. Ed. **55**, 7747 (2016).
[25]Y. F. Liang, L. Massignan, W. Liu, and L. Ackermann, Chem. - Eur. J. **22**, 14856 (2016).
[26]S.-Y. Chen, X.-L. Han, J.-Q. Wu, Q. Li, Y. Chen, and H. Wang, Angew. Chem., Int. Ed. **56**, 9939 (2017).
[27]J. B. Eastwood, T. J. Burden, L. A. Hammarback, C. Horbaczewskyj, T. F. N. Tanner, I. P. Clark, G. Greetham, M. Towrie, I. J. S. Fairlamb, and J. M. Lynam, Chem. Sci. **15**, 9183 (2024).
[28]C. R. Baiz, R. McCanne, M. J. Nee, and K. J. Kubarych, J. Phys. Chem. A **113**, 8907 (2009).
[29]M. J. Feng, F. Yang, and J. P. Wang, Chin. J. Chem. Phys. **29**, 81 (2016).
[30]S. Yan, M. T. Seidel, Z. Zhang, W. K. Leong, and H. S. Tan, J. Chem. Phys. **135**, 024501 (2011).
[31]V. F. Crum, L. M. Kiefer, and K. J. Kubarych, J. Chem. Phys. **155**, 134502 (2021).
[32]M. Delor, I. V. Sazanovich, M. Towrie, S. J. Spall, T. Keane, A. J. Blake, C. Wilson, A. J. H. M. Meijer, and J. A. Weinstein, J. Phys. Chem. B **118**, 11781 (2014).
[33]B. H. Jones, C. J. Huber, and A. M. Massari, J. Phys. Chem. C **115**, 24813 (2011).
[34]L. M. Kiefer and K. J. Kubarych, J. Phys. Chem. A **119**, 959 (2015).
[35]J. T. King, J. M. Anna, and K. J. Kubarych, Phys. Chem. Chem. Phys. **13**, 5579 (2011).
[36]J. T. King, M. R. Ross, and K. J. Kubarych, J. Phys. Chem. B **116**, 3754 (2012).
[37]M. Okuda, K. Ohta, and K. Tominaga, J. Phys. Chem. A **122**, 946 (2018).
[38]P. A. Eckert and K. J. Kubarych, J. Phys. Chem. A **121**, 608 (2017).
[39]L. M. Kiefer and K. J. Kubarych, Chem. Sci. **9**, 1527 (2018).
[40]V. F. Crum and K. J. Kubarych, J. Chem. Phys. **161**, 044507 (2024).
[41]P. W. J. M. Frederix, R. Kania, J. A. Wright, D. A. Lamprou, R. V. Ulijn, C. J. Pickett, and N. T. Hunt, Dalton Trans. **41**, 13112 (2012).
[42]R. Kania, A. I. Stewart, I. P. Clark, G. M. Greetham, A. W. Parker, M. Towrie, and N. T. Hunt, Phys. Chem. Chem. Phys. **12**, 1051 (2010).
[43]A. I. Stewart, J. A. Wright, G. M. Greetham, S. Kaziannis, S. Santabarbara, M. Towrie, A. W. Parker, C. J. Pickett, and N. T. Hunt, Inorg. Chem. **49**, 9563 (2010).
[44]J. C. Owrutsky and A. P. Baronavski, J. Chem. Phys. **105**, 9864 (1996).
[45]D. A. Steinhurst, A. P. Baronavski, and J. C. Owrutsky, Chem. Phys. Lett. **361**, 513 (2002).
[46]J. Z. Zhang and C. B. Harris, J. Chem. Phys. **95**, 4024 (1991).
[47]S. P. Church, H. Hermann, F.-W. Grevels, and K. Schaffner, J. Chem. Soc., Chem. Commun. **1984**, 785–786.
[48]R. S. Herrick and T. L. Brown, Inorg. Chem. **23**, 4550 (1984).
[49]T. Kobayashi, H. Ohtani, H. Noda, S. Teratani, H. Yamazaki, and K. Yasufukulc, Organometallics **5**, 110 (1986).
[50]P. Hamm and M. T. Zanni, *Concepts and Methods of 2D Infrared Spectroscopy* (Cambridge University Press, 2011).
[51]C. R. Baiz, P. L. McRobbie, N. K. Preketes, K. J. Kubarych, and E. Geva, J. Phys. Chem. A **113**, 9617 (2009).
[52]J. T. King, C. R. Baiz, and K. J. Kubarych, J. Phys. Chem. A **114**, 10590 (2010).
[53]M. J. Nee, C. R. Baiz, J. M. Anna, R. McCanne, and K. J. Kubarych, J. Chem. Phys. **129**, 084503 (2008).
[54]D. G. Osborne, J. T. King, J. A. Dunbar, A. M. White, and K. J. Kubarych, J. Chem. Phys. **138**, 144501 (2013).
[55]J. B. Eastwood, B. Procacci, S. Gurung, J. M. Lynam, and N. T. Hunt, ACS Phys. Chem. Au **4**, 536 (2024).
[56]L. P. DeFlores, R. A. Nicodemus, and A. Tokmakoff, Opt. Lett. **32**, 2966 (2007).
[57]S. H. Shim and M. T. Zanni, Phys. Chem. Chem. Phys. **11**, 748 (2009).
[58]F. A. Kvietok and B. E. Bursten, Organometallics **14**, 2395 (1995).
[59]C. R. Baiz, P. L. McRobbie, J. M. Anna, E. Geva, and K. J. Kubarych, Acc. Chem. Res. **42**, 1395 (2009).
[60]D. J. Parker and M. H. B. Stiddard, J. Chem. Soc. A **1966**, 695–699.
[61]N. J. Gould and D. J. Parker, Spectrochim. Acta, Part A **31**, 1785 (1975).
[62]D. J. Parker, Spectrochim. Acta, Part A **39**, 463 (1983).
[63]D. M. Adams, M. A. Hooper, and A. Squire, J. Chem. Soc. A **1966**, 695–699.
[64]W. T. Wozniak and R. K. Sheline, J. Inorg. Nucl. Chem. **34**, 3765 (1972).
[65]L. R. Snyder, J. Chromatogr. A **92**, 223 (1974).
[66]G. M. Sando, Q. Zhong, and J. C. Owrutsky, J. Chem. Phys. **121**, 2158 (2004).
[67]S. Kim, S. Park, S. K. Lee, and M. Lim, Chem. Phys. **487**, 37 (2017).
[68]M. Okuda, K. Ohta, and K. Tominaga, J. Chem. Phys. **145**, 114503 (2016).
[69]A. Tokmakoff, R. S. Urdahl, D. Zimdars, R. S. Francis, A. S. Kwok, and M. D. Fayer, J. Chem. Phys. **102**, 3919 (1995).
[70]M. Banno, K. Ohta, S. Yamaguchi, S. Hirai, and K. Tominaga, Acc. Chem. Res. **42**, 1259 (2009).
[71]R. M. Hochstrasser, M. A. Pereira, P. E. Share, M. J. Sarisky, Y. R. Kim, S. T. Repinec, R. J. Sension, J. R. G. Thorne, M. Iannone, R. Diller, P. A. Anfinrud, C. Han, T. Lian, and B. Locke, Proc. - Indian Acad. Sci. **103**, 351 (1991).
[72]Q. Guo, P. Pagano, Y. L. Li, A. Kohen, and C. M. Cheatum, J. Chem. Phys. **142**, 212427 (2015).
[73]D. G. Kuroda, K. S. Prabhat, and R. M. Hochstrasser, J. Phys. Chem. B **117**, 4354 (2013).
[74]Y. Wu, P. Yu, Y. Chen, J. Zhao, H. Liu, Y. Li, and J. Wang, J. Phys. Chem. Lett. **10**, 1402 (2019).
[75]M. Banno, K. Iwata, and H.-o. Hamaguchi, J. Chem. Phys. **126**, 204501 (2007).
[76]K. K. Lee, K. H. Park, C. Joo, H. J. Kwon, H. Han, J. H. Ha, S. Park, and M. Cho, Chem. Phys. **396**, 23 (2012).
[77]Y. L. A. Rezus, D. Madsen, and H. J. Bakker, J. Chem. Phys. **121**, 10599 (2004).
[78]C. Lee, H. Son, and S. Park, J. Phys. Chem. B **120**, 9723 (2016).
[79]H. Kim, S. Park, and M. Cho, Phys. Chem. Chem. Phys. **14**, 6233 (2012).
[80]J. C. Owrutsky, D. Raftery, and R. M. Hochstrasser, Annu. Rev. Phys. Chem. **45**, 519 (1994).
[81]T. Uzer and W. H. Miller, Phys. Rep. **199**, 73 (1991).
[82]P. A. Eckert and K. J. Kubarych, J. Phys. Chem. A **121**, 2896 (2017).
[83]F. Yang, X. Dong, M. Feng, J. Zhao, and J. Wang, Phys. Chem. Chem. Phys. **20**, 3637 (2018).

[84]D. V. Kurochkin, S. R. G. Naraharisetty, and I. V. Rubtsov, Proc. Natl. Acad. Sci. U. S. A. **104**, 14209 (2007).
[85]A. Pigliucci, G. Duvanel, L. M. L. Daku, and E. Vauthey, J. Phys. Chem. A **111**, 6135 (2007).
[86]T. Kiba, S. I. Sato, S. Akimoto, T. Kasajima, and I. Yamazaki, J. Photochem. Photobiol., A **178**, 201 (2006).
[87]A. I. Stewart, I. P. Clark, M. Towrie, S. K. Ibrahim, A. W. Parker, C. J. Pickett, and N. T. Hunt, J. Phys. Chem. B **112**, 10023 (2008).
[88]G. M. Bonner, A. R. Ridley, S. K. Ibrahim, C. J. Pickett, and N. T. Hunt, Faraday Discuss. **145**, 429 (2010).
[89]Q. Zhong and J. T. Fourkas, J. Phys. Chem. B **112**, 8656 (2008).
[90]N. T. Hunt, A. R. Turner, and K. Wynne, J. Phys. Chem. B **109**, 19008 (2005).
[91]J. R. Rajian, B. R. Hyun, and E. L. Quitevis, J. Phys. Chem. A **108**, 10107 (2004).
[92]P. W. J. M. Frederix, K. Adamczyk, J. A. Wright, T. Tuttle, R. V. Ulijn, C. J. Pickett, and N. T. Hunt, Organometallics **33**, 5888 (2014).
[93]T. Elsaesser and W. Kaiser, Annu. Rev. Phys. Chem. **42**, 83 (1991).
[94]D. W. Oxtoby, Annu. Rev. Phys. Chem. **32**, 77 (1981).
[95]M. Li, J. Owrutsky, M. Sarisky, J. P. Culver, A. Yodh, and R. M. Hochstrasser, J. Chem. Phys. **98**, 5499 (1993).
[96]C. Houchins, D. Weidinger, and J. C. Owrutsky, J. Phys. Chem. A **114**, 6569 (2010).